Investigation of Causes of Geometric Distortion in 180° and 360° Angular Sampling in SPECT

Karin Knešaurek, Michael A. King, Stephen J. Glick, and Bill C. Penney

Department of Nuclear Medicine, University of Massachusetts Medical Center, Worcester, Massachusetts

To investigate geometric distortion when 180° or 360° angular sampling techniques are used in single photon emission computed tomography (SPECT), a study of point sources imaged at different positions in a water filled cylindrical phantom, and reconstructed using filtered back projection, was conducted. A simulation study, based upon a serial model of the system point spread function (PSF), was used to investigate the contributions of attenuation, spatial resolution and scatter on distortion of the reconstructed PSFs. To study the geometric distortion in transverse (x-y plane), coronal (x-z plane), and sagittal (y-z plane) sections, the ratios of the full widths at half maximum (FWHM) and full widths at tenth maximum (FWTM) in the x/y, x/z, and y/z directions were calculated for the real and simulated PSFs. These results showed that, in an attenuating medium, there is more distortion of point sources into ovals for 180° than for 360° sampling. The simulation study indicated that the primary cause of geometrical distortion in SPECT studies, is the inconsistency of projections due to variable attenuation and spatial resolution. The impact of scatter on geometric distortion was small as measured by the ratios of FWHMs and FWTMs for PSFs. Attenuation correction applied to acquired PSFs significantly reduced geometric distortion in both 180° and 360° studies. To investigate distortion in extended objects, an Iowa heart phantom was placed inside an Alderson body phantom and ^{201}Tl heart SPECT studies acquired. The phantom images confirmed the conclusion that in transverse sections of 360° studies with arithmetic averaging of opposite views, geometric distortion is reduced compared to 180° studies. The coronal and sagittal sections were equally distorted in both, the 180° and 360° studies, and the 180° studies yielded better contrast.

J Nucl Med 30:1666–1675, 1989

In some recent comparison studies of 180° and 360° angular sampling in single photon emission computed tomography (SPECT) (*1–6*), it has been shown that reconstructed sections suffered from geometric distortion, especially in the 180° studies. One hundred eighty-degree SPECT angular sampling has been used, for the most part, in thallium-201 (^{201}Tl) myocardial imaging (*1,2,5*), but it has also been applied in liver and spleen studies (*4*). The advantages of 180° sampling in SPECT are shorter acquisition time if the same time per frame is used, better image contrast and, in some cases, better spatial resolution. The disadvantage of 180° sampling in SPECT is that it is not possible to average opposite views. As a consequence, the reconstructed image may suffer more severely than 360° angular sampling from geometric distortion.

To investigate geometric distortion in 180° and 360° SPECT imaging, both actual and simulated point source studies were used. A nonstationary, analytic simulation based upon a serial model (*7*) of the system point spread function (PSF) was used to separate the contributions of attenuation, spatial resolution, and scatter on the distortion of the reconstructed PSFs. These effects coupled with the reconstruction process itself produce the geometric distortion in the slice. Attenuation correction which uses a priori knowledge of the point source position was applied to real PSFs reducing significantly geometric distortion. Acquisitions of a ^{201}Tl myocardial phantom were taken and used to investigate geometric distortion in an extended object of known shape, in 360° and 180° SPECT studies.

Received June 29, 1988; revision accepted June 30, 1989.

For reprints contact: K. Knešaurek, PhD, Div. of Nuclear Medicine, Box 620, University of Rochester Medical Center, 601 Elmwood Ave., Rochester NY 14642.

MATERIALS AND METHODS

A single-headed, large field-of-view gamma camera (Dyna-Scan 5C, Picker International, Cleveland, OH) with a high-

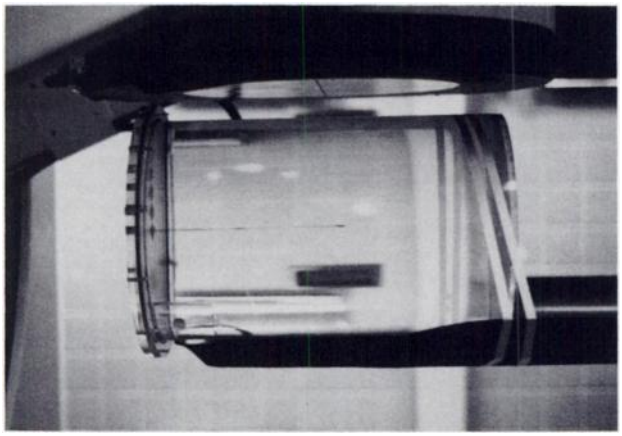

FIGURE 1
Cylinder 15.2 cm in radius filled with water used for acquisition of projection PSFs. At the top of the cylinder there were eight screws. Each screw had a small hole in the center which enabled penetration of a 30 cm long, 1.0 mm diameter, glass tube. One end of the glass tube was filled with highly concentrated solution of ^{99m}Tc activity.

resolution, low-energy parallel-hole collimator was used for acquisition of both point source and phantom studies. Data acquisition was performed with 15% energy window for point sources and a 25% energy window for ^{201}Tl heart phantom studies, in the "step and shoot" mode. 128 views over 360° were used for point source imaging. Each frame was stored as a 64 × 64 matrix. Image reconstruction was performed using software written on-site for a multiuser computer system (VAX 11/750, Digital Equipment Corporation, Marlboro, MA) with an array processor (Analogic, AP 500 Array Processor). Routine uniformity and center of rotation checks were performed. Pixel size was 0.58 cm and the thickness of the reconstructed section was 1 pixel wide. Prior to backprojection for 360° sampling, opposite frames were arithmetically averaged. No scatter correction was used. Only circular acquisitions with radius of rotation of 23 cm were performed. Backprojection reconstruction with ramp filtering was used for reconstructing the PSFs. In the phantom studies, in addition to the ramp filter, low-pass filtering was also applied (*8*).

Point Source Measurements

SPECT acquisitions of point sources at various locations in a water filled cylinder of radius 15.2 cm, was used to investigate the change in shape of reconstructed PSFs with position and method of angular sampling. At the top of the cylinder, starting from the center, there were eight screws, each with a small hole which enabled a 1.0-mm diameter glass tube to be inserted inside the cylinder (Fig. 1). The tube was 30 cm long and contained a drop of highly concentrated technetium-99m (^{99m}Tc) in one end. The length of the drop was 2 to 4 mm. The activities of the point sources were measured prior to acquisition and were within the range of 74–111 MBq (2–3 mCi). With this arrangement it was possible to place point sources within the water-filled cylinder at any desired depth with increments of 2 cm from the center. Each PSF was acquired separately, although the design of our phantom enables simultaneous acquisition of 8 point sources. Acquisition of each PSF separately was done to prevent mutual influence of point sources in our study. Each SPECT frame was acquired for 20 to 30 sec yielding ~30 000 counts per acquisition frame, when the source was at the center of the cylinder.

Reconstruction of 180° Sections in PSFs Studies

All point source studies were acquired as full 360° studies. From these, the software allowed the selection of any 180° arc for reconstruction of slices. It was thus possible to use the same acquisition data to reconstruct using all the projections to produce a slice, or only half of them covering any desired 180° arc. For the cylinder with a circular cross-section, and a circular orbit of rotation, any 180° segment could be chosen for study and the results could then be generalized to be true for any other segment, with appropriate rotation. Thus, for convenience, it was chosen to study the PSFs resulting from 180° acquisition centered about the x-axis. This leads to symmetric sampling of points on the x-axis, and asymmetric sampling of all other points. The specific 180° rotation which was modeled was that of rotating from 180°–0° (POS-ANT) as shown in Figure 2A.

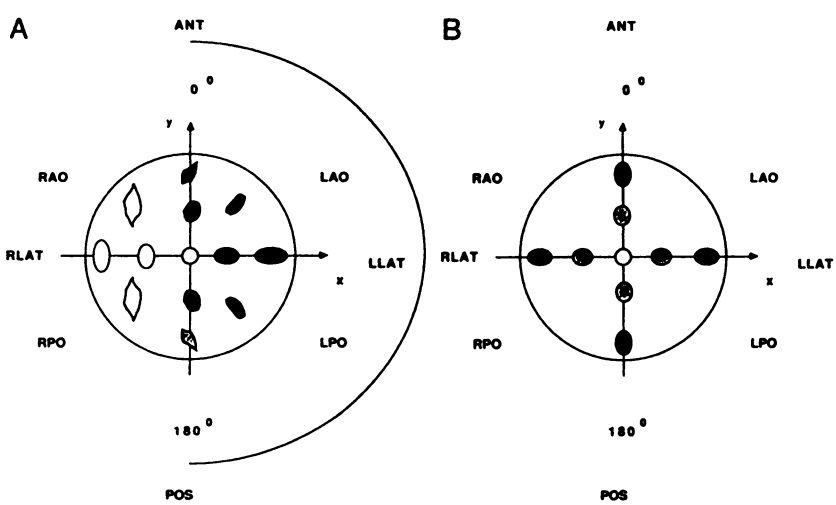

FIGURE 2
A: Reconstructed PSFs for 180°–0° (POS-ANT) study have a symmetrical shape for points on the x-axis and asymmetrical shape for all other points. The different intensities are represented using darker shadows for stronger points and lighter for weaker ones. This image does not give real proportions and true shapes, but rather shows the tendency of changing the shape and intensity of reconstructed PSFs at different positions, and the terminology used in describing source position. B: The same as for Figure 2A, but for 360° study with arithmetic averaging of opposing views. The image is radial symmetric.

Investigation of Geometric Distortion and Measurements of FWHM and FWTM

To study the geometric distortion and the variation in spatial resolution as a function of position within a slice, measurement of the full width at half maximum (FWHM) and the full width at tenth maximum (FWTM) of the PSFs was made. The shape of the reconstructed PSF in a transverse slice, was described by FWHM and FWTM along the x- and y-axis. The ratio $FWHM_x/FWHM_y$, as shorten to $FWHM_{x/y}$, and the ratio $FWTM_x/FWTM_y$, as shorten to $FWTM_{x/y}$, were used to investigate the geometrical distortion of the reconstructed PSFs at different positions in transverse slice. The same was done for sagittal and coronal sections using corresponding ratios, i.e., $FWHM_{x/z}$, and $FWTM_{x/z}$ for coronal sections, and $FWHM_{y/z}$ and $FWTM_{y/z}$ for sagittal sections. For symmetrically sampled points (points on x-axis of Fig. 2A) calculation of FWHM was performed by fitting the x, y, and z axes profiles of the PSFs with a Gaussian function. A single Gaussian function accurately models only the central part of the PSF in a scattering medium. So, the Gaussian fit was not used for the calculation of the FWTM. Instead linear interpolation was used to determine the position of one-tenth the Gaussian fit maximum. Such values of the FWTM were slightly higher than those obtained from the fit to Gaussian function because of the contribution of the scattering "tails".

For PSFs not symmetrically sampled, calculation of the FWHM and FWTM in the radial and tangential directions, was much more difficult. These PSFs were rotated to align their "semi-major" and "semi-minor" axis with the horizontal x-axis and vertical y-axis, respectively and the FWHM and FWTM were calculated as for those points on the x-axis (*9*). Bilinear interpolation was used to rotate the PSFs.

Simulation Study

To independently assess the contributions of spatial resolution, attenuation and scatter on geometric distortion of point sources, a simulation study based upon a serial model of the system PSF (*7,10,11*) was employed. The serial model has the advantage of separating the depth dependent scattering component and distance dependent geometric component of the total PSF. The geometric component was modeled as a single Gaussian function whose FWHM is linear function of the distance from the collimator (*6,10*). This dependence was determined from point source measurements in air for our system. The scattering component was modeled as the convolution of the geometric response for the given distance and a second Gaussian whose FWHM varied as a function of source depth. The relationship between FWHM and depth for the second Gaussian was determined from point source measurements in water and was in good agreement with previously published results (*7*). The scatter component was scaled by the scatter fraction (SF) for a point at the desired depth and added to the geometric response. The SF was obtained from a regression equation based on values of SF measured on our system (*12*). The sum of the primary and scatter components was then scaled by an attenuation factor for the particular depth. The attenuation factor was calculated using the "good geometry" value of the linear attenuation coefficient, since "buildup" was included in the scatter component.

An analytic approach was used to calculate projections.

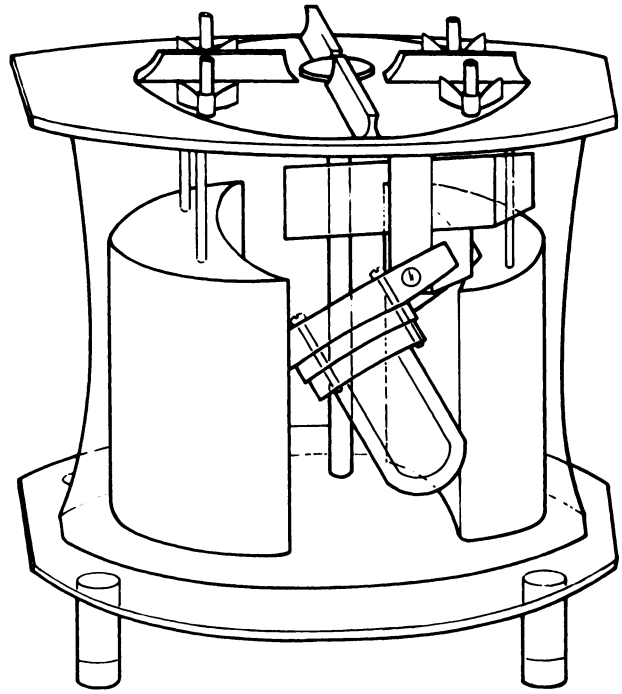

FIGURE 3
The combination of the Alderson body, and the "Iowa" heart phantom was used to mimic ^{201}Tl heart SPECT studies. In the Alderson phantom, surrounding the "Iowa" heart phantom, were placed styrofoam "lungs" and nylon rod 2 cm in diameter to simulate the spine.

TABLE 1
FWHMs and Corresponding Ratios for Transverse (x-y), Coronal (x-z), and Sagittal (y-z) Planes for Point Sources Located on the x-Axis of Figure 2A for 180°-0° (POS-ANT) Study

Distance along x-axis (cm)	FWHM (cm) x-axis	y-axis	z-axis	$FWHM_{x/y}$	$FWHM_{x/z}$	$FWHM_{y/z}$
−14	1.41	7.17	2.32	0.20	0.61	3.09
−12	1.40	7.65	2.01	0.18	0.70	3.81
−8	1.52	3.98	2.12	0.38	0.72	1.88
−4	1.71	2.62	2.05	0.65	0.83	1.23
0	1.90	2.00	1.96	0.95	0.97	1.02
4	2.16	1.67	1.86	1.23	1.16	0.90
8	2.20	1.44	1.76	1.52	1.25	0.82
12	2.13	1.17	1.50	1.82	1.42	0.78
14	2.05	1.19	1.50	1.72	1.38	0.79

TABLE 2
FWTMs and Corresponding Ratios for Transverse (x-y), Coronal (x-z), and Sagittal (y-z) Planes for Point Sources Located on the x-Axis of Figure 2A for 180°-0° (POS-ANT) Study

Distance along x-axis (cm)	FWTM (cm) x-axis	y-axis	z-axis	$FWTM_{x/y}$	$FWTM_{x/z}$	$FWTM_{y/z}$
−14	2.56	***	***	***	***	***
−12	2.55	***	3.68	***	0.68	***
−8	2.77	8.57	3.87	0.32	0.72	2.21
−4	3.11	5.08	3.74	0.61	0.83	1.36
0	3.48	3.70	3.57	0.94	0.97	1.04
4	3.96	3.04	3.39	1.30	1.17	0.90
8	4.06	2.62	3.20	1.55	1.27	0.82
12	3.94	2.13	2.73	1.85	1.44	0.78
14	3.73	2.16	2.74	1.74	1.37	0.79

*** Denotes that FWTM was below background.

The activity associated with a given position was first blurred with the symmetrical PSF distribution, as calculated above, and then sampled. This approach has the advantages that aliasing effects are significantly reduced and projection values are calculated analytically without using interpolation (*13*). The simulation study also allowed the introduction of different levels of Poisson noise in the noise-free projections (*14*).

The analytic, nonstationary simulation was tested by comparing the predicted planar and SPECT PSFs with those actually acquired on the system and was used to (a) investigate geometric distortion associated with 180° and 360° angular sampling as a function of source location (b) to investigate the contribution of each effect, i.e., attenuation, spatial resolution and scattering, separately, and (c) to investigate noise effects on the quality of the reconstructed PSFs. To reduce aliasing in images reconstructed when no resolution effects were included in the simulation, a Gaussian distribution of the activity was assumed within $\sigma = 0.5$ pixel.

Thallium-201 Heart Phantom Study Acquisitions

The combination of two standard phantoms was used to simulate clinical heart studies (Fig. 3.). One was the "Iowa" heart phantom (Data Spectrum Corporation, Chapel Hill, NC), which consisted of two chambers and simulated the left ventricle. The inside of the inner chamber is used to model left ventricular cavity and was filled with water. The space between the inner and outer chambers models the "ventricle wall". Within this space an activity of 37 MBq (1 mCi) of ^{201}Tl was uniformity distributed. The "Iowa" heart phantom was surrounded by styrofoam "lungs" and placed inside the Alderson organ scanning phantom (Alderson Research Laboratories Inc., Stamford, CT), which simulated the body (*15*). Also, a nylon rod of radius 2 cm was placed inside the Alderson phantom to simulate spine (*16*). Remaining space in body phantom was filled with water. Two studies were acquired, both with the same total time of the acquisition. One was a standard 180° acquisition with 32 views, 180 sec each. Another was a 360° acquisition with 64 views, 90 sec each, yielding approximately one half the counts per projection. The total number of counts in each projection depended on projection angle and ranged from 55 to 17 thousand counts in the 360° study.

RESULTS

In Table 1 are presented the FWHMs and ratios $FWHM_{x/y}$, for reconstructed point sources along the x-axis of the cylinder (see Fig. 2A) as reconstructed with 180° sampling centered about x-axis. In Table 2 the corresponding FWTMs and $FWTM_{x/y}$ are tabulated. Table 1 and Table 2 show that in the transverse section, the shape of the PSF changes significantly versus x-axis position. This is portrayed in Figure 2A where the points are shown to change from vertical to horizontal ellipses as one precedes along the axis of symmetry. The actual PSFs in transverse section reconstructed at three of these locations are presented in Figure 4. Tables 1 and 2 show that although resolution in the direction perpendicular to the axis of symmetry (the y direction in Fig. 2A) improves as the point moves closer to the detector, resolution along the x-axis degrades. Similar trends are noted as one moves from the center of the phantom out to the edge with 360° sampling and using

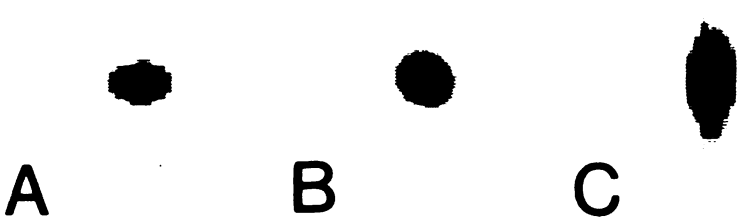

FIGURE 4
Symmetric PSFs for 180°–0° (POS-ANT) study. A: Reconstructed PSF at x = 8 cm or LLAT position. B: Reconstructed PSF at the center, x = 0 cm. C: Reconstructed PSF at x = −8 cm or RLAT position.

TABLE 3
FWHMs and Corresponding Ratios for Transverse (x-y), Coronal (x-z) and Sagittal (y-z) Planes, for Point Sources Located on the x-Axis of Figure 2B for a 360° Study with Arithmetic Averaging of Opposing Projections*

Distance along x-axis (cm)	FWHM (cm) x-axis	y-axis	z-axis	$FWHM_{x/y}$	$FWHM_{x/z}$	$FWHM_{y/z}$
0	1.93	1.97	1.96	0.98	0.98	1.00
4	2.04	1.82	1.91	1.12	1.07	0.95
8	2.09	1.55	1.81	1.35	1.15	0.86
12	2.09	1.22	1.52	1.71	1.38	0.80
14	2.01	1.23	1.53	1.63	1.31	0.80

* Because of the symmetry with 360° sampling, negative x-axis locations are not shown.

the arithmetic mean to combine opposing views (Table 3, Table 4, and Fig. 2B). However, for 360° reconstruction, the ratios $FWHM_{x/y}$ and $FWTM_{x/y}$ are closer to 1.0 than with 180° reconstruction. These results show that geometric distortion in transverse sections will be worse for 180° than 360° acquisitions.

In Table 5 and Table 6 are given the FWHM, FWTM and corresponding ratios for asymmetrically sampled points (LAO, ANT, RAO) displaced 8 cm from the center of rotation (approximately one-half way from the center to the edge). These points are also significantly distorted. Their shape is no longer elliptical (*6*) as is shown in Figure 2A and by the actual PSFs in Figure 5.

The direction of PSFs distortion ('semi-major' axis) in the 180° studies in transverse sections depends on the position of the point source. Definition of systematic relationship between distortion direction and starting angle of data sampling is difficult (*17*), especially for distant asymmetric points, i.e., in our case for left side points which are not on x-axis (Fig. 2A).

The main object of this study was to investigate the geometrical distortion in the transverse sections, because sagittal and coronal sections are obtained from them. However, the results of our studies indicate that investigation of geometrical distortion in the coronal and sagittal plane is also necessary. The results presented in Tables 1–4, show that 180° sections have more geometrical distortion than the same 360° sections. However, in the clinically interesting region (i.e., for the points on the right side on Fig. 2A), geometric distortion is less expressed in coronal and sagittal sections than in the transverse sections. Also, in this region the ratios $FWHM_{x/z}$ and $FWHM_{y/z}$ for 180° and 360° SPECT studies are quite close, indicating that a similar amount of the geometric distortion would appear in the coronal and sagittal sections for both the angular sampling methods.

The advantage of using simulation studies over patient or phantom data is that each effect, e.g., variations in attenuation, scatter, spatial resolution, and noise, can be investigated separately. Also the "truth", i.e., the starting object, is known and can be used as a reference.

The point sources in the clinically interesting area, i.e., on the positive x-axis in Fig. 2A, were chosen for the simulation study. The central point was not distorted and was omitted from the tables. In Table 7 and Table 8 are presented the results of the simulation study for 180° and 360° studies. Again, angular sampling from 180°–0° (POS-ANT), as shown in Figure 2A, was used for 180° study, as well as the radius of rotation of the gamma camera equal to 23 cm and the radius of the attenuating cylinder equal to 15.2 cm. These acquisition parameters were chosen to allow comparison of the experimentally obtained ratios $FWHM_{x/y}$, $FWHM_{x/z}$ and $FWHM_{y/z}$ (Tables 1 and 3) with those obtained from the simulation study which included all effects (Tables 7 and 8). The comparison has shown good

TABLE 4
FWTMs and Corresponding Ratios for Transverse (x-y), Coronal (x-z), and Sagittal (y-z) Planes, for Point Sources Located on the x-Axis of Figure 2B for a 360° Study with Arithmetic Averaging of Opposing Projections*

Distance along x-axis (cm)	FWTM (cm) x-axis	y-axis	z-axis	$FWTM_{x/y}$	$FWTM_{x/z}$	$FWTM_{y/z}$
0	3.52	3.60	3.58	0.98	0.98	1.00
4	3.73	3.31	3.49	1.13	1.07	0.95
8	3.85	2.83	3.29	1.36	1.17	0.86
12	3.86	2.21	2.77	1.75	1.39	0.80
14	3.67	2.24	2.78	1.64	1.32	0.81

* Because of the symmetry with 360° sampling, negative x-axis locations are not shown.

TABLE 5
FWHMs and Corresponding Ratios for Point Sources Located at 8-cm Distance from the Center at Points Other Than the x-Axis of Figure 2A for a 180°-0° (POS-ANT) study*

Position	FWHM (cm) M-axis	m-axis	z-axis	$FWHM_{M/m}$	$FWHM_{M/z}$	$FWHM_{m/z}$
LAO	2.60	1.29	1.76	2.02	1.48	0.73
ANT	2.25	1.14	1.81	1.97	1.24	0.63
RAO	4.90	1.15	1.98	4.26	2.47	0.58

* The semi-major axis is denoted M-axis and semi-minor as m-axis.

agreement between ratios obtained from experimental and simulated data.

The results shown in Tables 7 and 8 demonstrate that the attenuation effects are the main cause of the geometric distortion in the both 180° and 360° studies, except for the the points close to the edge of the attenuating medium. The resolution effects are also significant, and for edge points they become the dominant cause of the geometric distortion. The influence of the scatter effects on the geometric distortion was quite small for both angular sampling techniques. The results also show that arithmetic averaging of opposing projections has a tendency to reduce nonuniformity in the projections due to attenuation and resolution effects, giving less distorted reconstructed PSFs. In Figure 6 are shown 180° and 360° PSFs at a position of x = 8 cm, reconstructed from simulated noise-free projections with attenuation, resolution and scattering effects taken into account. The PSF reconstructed from experimentally acquired projections is shown on Figure 4A. The PSF obtained using a simulated 180° study is "pressed" by negative values from above and below (Fig. 6A B). The same effect was significantly reduced in a 360° study (Fig. 6C and D).

In Figure 7 are shown transverse sections of a simulated 180° study of a point source at the same location as in Figure 6. In Figure 7A the PSF is reconstructed from ideal projections, i.e., none of the effects were taken into account, in Figure 7B from projections effected by attenuation only, in Figure 7C effected by resolution only, and in Figure 7D effected by scattering only. The negative values seen above and below the reconstructed PSF on Figure 7B are due to attenuation effects.

The simulation study indicates that attenuation correction should significantly reduce geometric distortion. To test this, the real PSFs were reconstructed with and without attenuation correction and the results were compared. Ideal pre-reconstruction attenuation correction, using a priori knowledge of the point source position was used (*18*). In Table 9 and 10 are presented results of the effects of the attenuation correction on the geometric distortion for 180° and 360° imaging, for the points on the positive x-axis locations. The comparison of the corresponding ratios from Table 1 and Table 3 with those given in Table 9 and Table 10 shows that attenuation correction significantly reduces geometric distortion in both the 180° and 360° studies. A reduction of the geometric distortion caused by attenuation correction is noted in all sections. The greatest reduction was observed in transverse sections and the smallest in the 180° sagittal sections. Here, attenuation correction was particularly effective in reducing the geometric distortion, for points up to one-half the phantom's radius from the center. In the 360° studies the geometric distortion was practically eliminated by this attenuation correction.

The number of counts in 180° studies in SPECT imaging is usually two or more times that in corresponding 360° studies due to longer acquisition time per frame and due to more attenuation on rear views. That leads to a better signal-to-noise ratio in 180°

TABLE 6
FWTMs and Corresponding Ratios for Point Sources Located at 8-cm Distance from the Center at Points Other Than the x-Axis of Figure 2A for a 180°-0° (POS-ANT) Study*

Position	FWTM (cm) M-axis	m-axis	z-axis	$FWTM_{M/m}$	$FWTM_{M/z}$	$FWTM_{m/z}$
LAO	4.88	2.35	3.21	2.08	1.52	0.73
ANT	4.16	2.08	3.31	2.00	1.26	0.63
RAO	9.30	2.09	3.62	4.45	2.57	0.58

* The semi-major axis is denoted M-axis and semi-minor as m-axis.

FIGURE 5
Asymmetric PSFs for 180°–0° (POS-ANT) study. A: Reconstructed PSF at 8 cm distance from the center, LAO position. B: Reconstructed PSF at 8 cm distance from the center, ANT position, y = 8 cm. C: Reconstructed PSF at 8 cm distance from the center, RAO position.

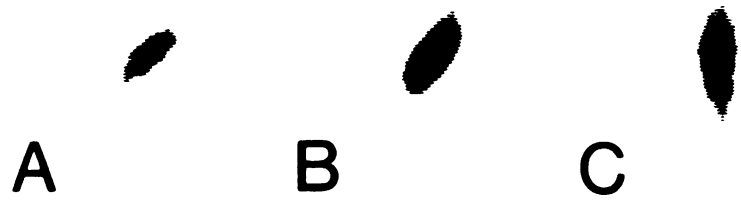

studies, but does not change the shape of the reconstructed object. To demonstrate that this claim is true, in addition to the noise-free simulation of the reconstructed PSF for 180° study shown on Figure 6A, the same PSFs, only with different amounts of noise were reconstructed (Fig. 8). The PSF shown on Figure 8A and B has three time less noise than other PSF shown on Figure 8C and D. In spite of this the corresponding FWHMs and FWTMs were practically the same.

Transverse sections of the ^{201}Tl "Iowa" heart phantom SPECT study, obtained from projections covering only 225°–45° arc and from projections covering all 360°, are shown on Figure 9A and B, respectively. In the second and third row are shown the corresponding coronal sections along the short axis (Fig. 9C and D) and sagittal sections along the vertical long axis (Fig. 9E and F), respectively. The advantage of using phantom over clinical studies is that source distribution and the geometry are known. Also the problems of motion and redistribution are avoided.

The results of our "Iowa" heart phantom SPECT studies show that in all 180° sections there is significantly better image contrast due to less attenuation in anterior projections. This study also shows that both 180° and 360° transverse sections suffer from geometrical distortion (*6*) (Fig. 9A and B). This distortion is expressed as changes in shape of the reconstructed images. However, it seems that 180° transverse section is slightly more distorted than the same 360° transverse section as measured to be the case for PSFs (Table 1–Table 4). The artifact seen in the apex region of the 180° transverse section (Fig. 9A) is also less expressed in the same region of the 360° transverse section (Fig. 9B). The same type of artifact, in the 180° transverse and sagittal sections, has been reported in ^{201}Tl clinical SPECT studies (*5*). Also, 360° transverse section seems to more closely follow the known "U" shape of the phantom slice (Fig. 9B).

The shapes of coronal sections along the short axis are quite circular for both the 360° and 180° studies (Fig. 9C and D), confirming the results of PSF analysis. Due to better image contrast, the 180° coronal sections provide sharper delineation of the left ventricular cavity and ventricular segments (*5*).

Sagittal sections (Fig. 9E and F) are almost equally distorted in both the 360° and 180° studies, because the "Iowa" phantom was placed close to 180° gamma camera orbit. Similar results were obtained for point sources in our study, which were placed in the clinically interesting area, i.e., on the right side in Figure 2A. Again in 180° heart phantom sagittal sections there is significantly better image contrast than in the same 360° sagittal sections.

DISCUSSION AND CONCLUSIONS

In the clinical situation with less attenuation anteriorly due to the lungs and the positioning of the heart, greater contrast and better spatial resolution in the tangential direction will be obtained with 180° sampling. However, the PSF, simulation, and "Iowa" heart phantom SPECT studies indicate that more shape distortion will occur with this mode of acquisition than 360° sampling. This is in agreement with previously reported results (*5,19*) of ^{201}Tl myocardial perfusion SPECT studies.

The spatial distortion seen in SPECT studies is the

TABLE 7
The Ratio $FWHM_{x/y}$ Calculated from Simulated PSFs Including Only Attenuation, Resolution, and Scattering Effects and Including All of These Effects, for 180°-0° (POS-ANT) Study

Position along x-axis (cm)	$FWHM_{x/y}$ Attenuation effects only	$FWHM_{x/y}$ Resolution effects only	$FWHM_{x/y}$ Scatter effects only	$FWHM_{x/y}$ All effects
4	1.24	1.10	0.91	1.34
8	2.26	1.23	0.94	1.64
12	3.73	1.46	0.99	1.84
14	1.23	1.49	0.93	1.69

TABLE 8
The Ratio $FWHM_{x/y}$ Calculated from Simulated PSFs Including Only Attenuation, Resolution, and Scattering Effects and Including All of These Effects, for 360° Study with Arithmetic Averaging of Opposite Projections

Position along x-axis (cm)	$FWHM_{x/y}$ Attenuation effects only	$FWHM_{x/y}$ Resolution effects only	$FWHM_{x/y}$ Scatter effects only	$FWHM_{x/y}$ All effects
4	1.00	1.01	0.91	1.12
8	1.13	1.05	0.94	1.40
12	1.18	1.17	0.99	1.65
14	0.95	1.20	0.93	1.55

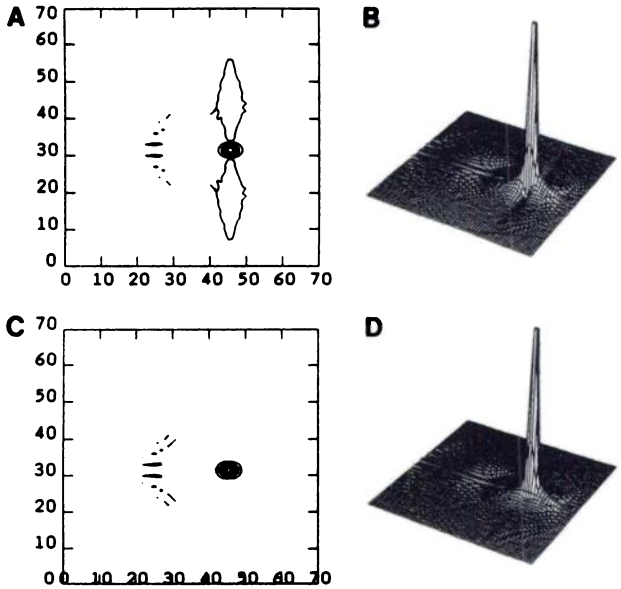

FIGURE 6
A, B: The contour and surface plot, respectively of the 180° reconstructed PSF at x = 8 cm or LLAT position, from simulated noise-free projections, with attenuation, resolution and scattering effects included. C, D: The same for 360° reconstructed PSF, with arithmetical averaging of opposing views.

result of the variable attenuation, of variable resolution with the distance from the collimator, and of depth dependent scatter, and of the reconstruction process itself. All of these effects (i.e., attenuation, spatial resolution and scatter) provide inconsistent projection data. Variable attenuation and scatter are caused not only by nonuniform attenuation within the object, but also by

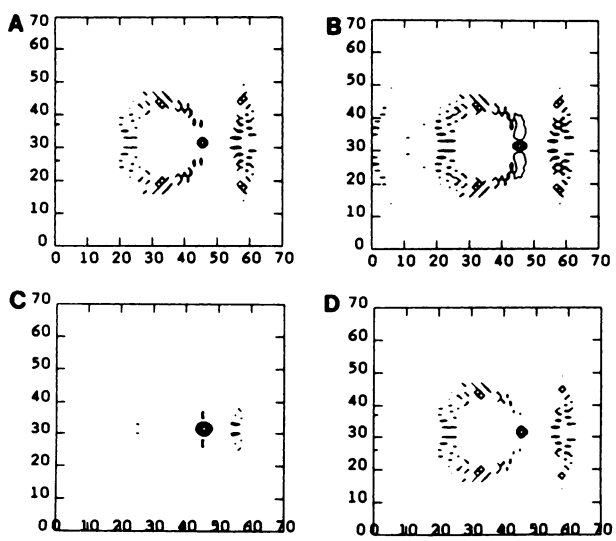

FIGURE 7
Reconstructed PSFs at x = 8 cm or LLAT position for 180°–0° (POS-ANT) study with (A) only filtered backprojection of ideal noise-free projections, (B) with only attenuation effects included, (C) with only resolution effects included, and (D) with only scattering effects included.

TABLE 9
FWHMs and Corresponding Ratios for Transverse (x-y), Coronal (x-z), and Sagittal (y-z) Planes for Point Sources Located on the Positive x-Axis Locations of Figure 2A for 180°-0° (POS-ANT) Studies, with Attenuation Correction

Distance along x-axis (cm)	FWHM (cm) x-axis	y-axis	z-axis	$FWHM_{x/y}$	$FWHM_{x/z}$	$FWHM_{y/z}$
4	2.06	1.73	1.86	1.19	1.11	0.93
8	2.02	1.53	1.77	1.32	1.14	0.86
12	2.00	1.23	1.51	1.63	1.32	0.81
14	1.93	1.24	1.51	1.55	1.28	0.82

different depths of active points in the media, as viewed from different projections (*16*).

In 360° sections obtained from a uniform attenuating media shape changes are less expressed as a function of position within the reconstructed image, due to averaging of opposing views. Thus, by averaging conjugate views, it is possible to preserve the shape and relative distances within the reconstructed objects to a greater extent than with 180° studies. The averaging of opposite views has the effect of correcting the projection values prior to filtered-backprojection. This pre-reconstruction correction helps to preserve sensitivity (*20*) and the shape of the reconstructed object. Without averaging of opposing views, the projection values are usually more distorted by attenuation, resolution and scatter effects. Also, the reconstruction process itself has a tendency to amplify these distortions in the projections, giving reconstructed images of poor quality. It is true that even with averaging of opposing projections reconstructed PSFs for off-center and distant point-sources turn to ovals. But this distortion, in a case of uniform attenuation, is less expressed in 360° studies as compared with 180°. In the real clinical situation with extended source geometries and with complex variation in attenuation, such as occur in thorax, 360° sampling may no longer yield less distorted reconstructions than 180° sampling.

The ramp filter introduces negative values into the projections. The backprojection of these negative values is used to cancel the false positive contributions from other angles. The assumption is that each projection

TABLE 10
FWHMs and Corresponding Ratios for Transverse (x-y), Coronal (x-z), and Sagittal (y-z) Planes for Point Sources Located on the x-Axis Locations of Figure 2B for 360° Studies with Arithmetic Averaging of Opposing Projections and with Attenuation Correction

Distance along x-axis (cm)	FWHM (cm) x-axis	y-axis	z-axis	$FWHM_{x/y}$	$FWHM_{x/z}$	$FWHM_{y/z}$
4	1.99	1.90	1.94	1.05	1.03	0.98
8	1.95	1.80	1.89	1.08	1.03	0.95
12	1.99	1.40	1.61	1.42	1.24	0.87
14	1.93	1.44	1.62	1.34	1.19	0.89

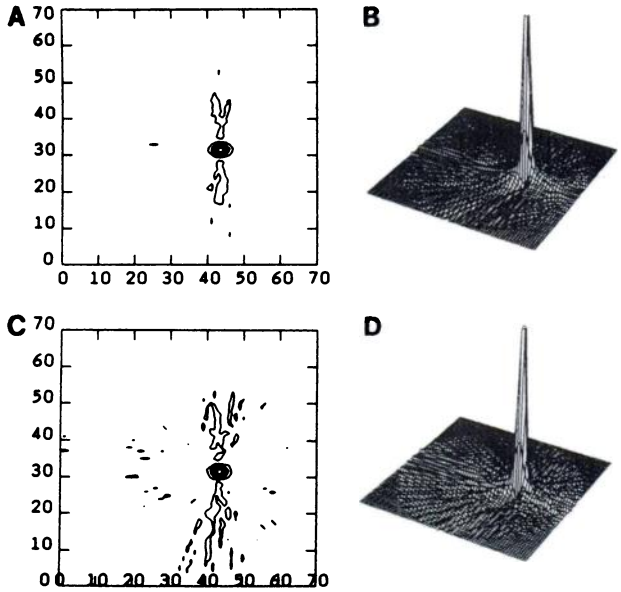

FIGURE 8
Investigation of the noise effects on the reconstructed PSFs at x = 8 cm or LLAT position for 180°–0° (POS-ANT) study. The PSF in A and B has ten times more counts, than the PSF shown of C and D. However, they have the same shape and the corresponding FWHMs and FWTMs are the same.

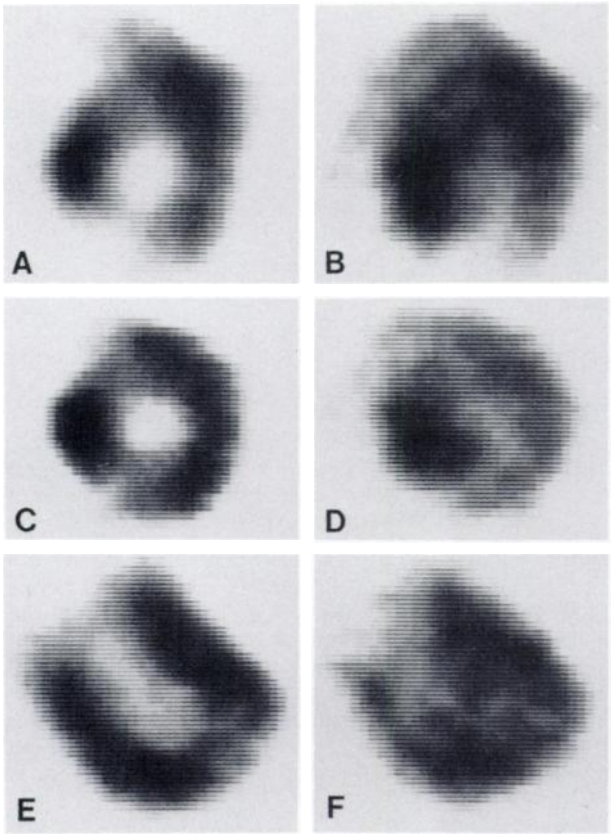

FIGURE 9
Sections obtained from ^{201}Tl "Iowa" heart phantom SPECT study. A: Transverse 180° section obtained from only projections covering an LPO-RAO (225°–45°) arc. B: The same 360° transversal section. C: 180° coronal section along the short axis. D: The same 360° coronal section as on C. E: 180° sagittal section along the vertical long axis. F: The same 360° sagittal section as on E.

represents a consistent sampling of the section to be reconstructed. That is, the negative values will cancel out the incorrect positive counts added to each pixel. Attenuation and scatter causes point source sensitivity to vary with the depth. Further, the variation in distance from collimator of each point in the image (except the center of rotation for circular orbits), results in each point being viewed with different resolution as the camera circles the patient. This results in the contribution of a point to the projection data to also vary with projection angle. Thus, the canceling of the positive and negative values is altered by variable attenuation (*16*), spatial resolution, and scatter. The result is the distortion seen in 180° sections and, to a lesser extent, in 360° studies.

In order to reduce the geometric distortion in SPECT imaging, particularly in 180° studies, attenuation, resolution, and scattering corrections should be employed (*15,21–26*).

ACKNOWLEDGMENTS

This work was supported in part by Centocor Corporation, the National Cancer Institute under grant CA42165 and by SIZ-za znanost SR Hrvatske, Yugoslavia. The authors also thank the reviewers for their valuable comments and suggestions.

REFERENCES

1. Coleman RE, Jaszczak RJ, Cobb FR. Comparison of 180° and 360° data collection in thallium-201 imaging using SPECT. *J Nucl Med* 1982; 23:655–660.
2. Tamaki N, Mukai T, Ishii Y, et al. Comparative study of thallium emission myocardial tomography with 180° and 360° data collection. *J Nucl Med* 1982; 23:661–666.
3. Hoffman EJ. 180° compared with 360° sampling in SPECT. *J Nucl Med* 1982; 23:745–747.
4. Ott RJ, Flower MA, Khan O, et al. Comparison between 180° and 360° data reconstruction in SPECT of the liver & spleen. *Br J Radiol* 1983; 56:931–937.
5. Go RT, MacIntyre WJ, Houser TS, et al. Clinical evaluation of 360° and 180° data sampling techniques for transaxial SPECT thallium-201 myocardial perfusion imaging. *J Nucl Med* 1985; 26:695–706.
6. Eisner RL, Nowak DJ, Pettigrew R, Fajman W. Fundamentals of 180° acquisition and reconstruction in SPECT imaging. *J Nucl Med* 1986; 27:1717–1728.
7. Atkins FB. Monte Carlo analysis of photon scattering in radionuclide imaging, 1978, Ph.D. Thesis, University of Chicago.
8. Knesaurek K, Spaventi S. The spatial resolution and noise in SPECT based on rotational gamma camera. In: Vogler E and Schneider GH, eds. *Digitale bildgebende verfahren integrierte digitale radiologie.* Berlin: Schering AG; 1986; 990–995.
9. Clausen M, Bice AN, Wagner HN. Resolution of line

sources in SPECT with 180° sampling. *Nucl Compact* 1985; 16:449–454.
10. Knešaurek K, King MA, Glick SJ, Penney BC. A 3-D non-stationary simulation of SPECT imaging [Abstract]. *J Nucl Med* 1989; 30:881.
11. Gilland DR, Tsui BMW, McCartney WH, Perry JR, Berg J. Determination of the optimum filter function for SPECT imaging. *J Nucl Med* 1988; 29:643–650.
12. Knešaurek K, King MA, Glick SJ. Two methods of scatter fraction measurement in SPECT imaging [Abstract]. *J Nucl Med* 1989; 30:876.
13. Glick SJ, King MA, Penney BC. Characterization of the MTF of discrete filtered backprojection. *IEEE Tran Med Imag*: in press.
14. Lo CM: Estimation of image signals with Poisson noise, 1979, Ph.D. Thesis, University of Southern California.
15. Tsui BMW, Gullberg GT, Edgerton ER et al. Correction of nonuniform attenuation in cardiac SPECT imaging. *J Nucl Med* 1989; 30:497–507
16. Manglos SH, Jaszczak RJ, Floyd CE, Hahn LJ, Greer KL, Coleman RE. Nonisotropic attenuation in SPECT: test of quantitative effects and comparison techniques. *J Nucl Med* 1987; 28:1584–1591.
17. Bice AN, Clausen M, Loncaric S, Wagner HN. Comparison of transaxial resolution in 180° and 360° SPECT with rotating scintillation camera. *Eur J Nucl Med* 1987; 13:7–11.
18. Glick SJ, King MA, Knesaurek K, Burbank K. An investigation of the stationarity of the 3D modulation transfer function of SPECT. *IEEE Nucl Sci* 1989; 36:973–977.
19. MacIntyre WJ, Go RT, O'Donnell JK, et al. Thallium-201 and technetium-99m pyrophosphate-single photon emission computed tomography. In: Gelfand MJ, Thomas SR, eds. *Effective use of computers in nuclear medicine.* New York: McGraw-Hill Inc, 1988: 109–135.
20. Knešaurek K. Comparison of 360° and 180° data collection in SPECT. *Phys Med Biol* 1987; 32:1445–1456.
21. Bailey DL, Hutton BF, Walker PJ. Improved SPECT using simultaneous emission and transmission tomography. *J Nucl Med* 1987; 28:844–851.
22. Tsui BMW, Hu HB, Gilland DR, Gullberg GT. Implementation of simultaneous attenuation and detector response correction in SPECT. *IEEE Trans Nucl Sci* 1988; 35:778–783.
23. Singh M, Horne M, Maneval D, Amartey J, Brecher R. Non-uniform attenuation and scatter correction in SPECT. *IEEE Trans Nucl Sci* 1988; 35:767–771.
24. Liang Z, Hart H. Bayesian reconstruction in emission computerized tomography. *IEEE Trans Nucl Sci* 1988; 35:788–792.
25. Floyd CE, Jaszczak RJ, Manglos SH, Coleman RE. Compensation for collimator divergence in SPECT using inverse Monte Carlo reconstruction. *IEEE Trans Nucl Sci* 1988; 35:784–787.
26. Tsui BMW, Zhao XD, Ballard JG, et al. Comparison of 180° and 360° reconstruction for cardiac SPECT imaging using Tl-201 and Tc-99m agents. [Abstract]. *J Nucl Med* 1989; 30:756.